Showcasing research undertaken by Dr. Chia-Yun Chen from the Laboratory for Energy Materials and Nanodevices, National Cheng Kung University, Taiwan.

Unveiling the detection kinetics and quantitative analysis of colorimetric sensing for sodium salts using surface-modified Au-nanoparticle probes

The ascorbic-acid treated gold-nanoparticle probes are presented that enable to activate the pronounced color change for detecing Na^+-ion contents visually.

As featured in:

See Chia-Yun Chen *et al.*, *Nanoscale Adv.*, 2022, **4**, 3172.

ROYAL SOCIETY OF CHEMISTRY

rsc.li/nanoscale-advances

Registered charity number: 207890

Nanoscale Advances

ROYAL SOCIETY OF CHEMISTRY

PAPER

View Article Online
View Journal | View Issue

Cite this: *Nanoscale Adv.*, 2022, **4**, 3172

Unveiling the detection kinetics and quantitative analysis of colorimetric sensing for sodium salts using surface-modified Au-nanoparticle probes†

Min Hsiao,[a] Shih-Hsiu Chen,[a] Jheng-Yi Li,[a] Po-Hsuan Hsiao[a] and Chia-Yun Chen *[ab]

Received 4th April 2022
Accepted 24th May 2022

DOI: 10.1039/d2na00211f

rsc.li/nanoscale-advances

Rapid, reliable, and sensitive colorimetric detection has been regarded as a highly potential technique for visually monitoring the cation ions. Yet, insight into detection kinetics and quantitative analysis for colorimetric sensing of sodium ions has rarely been revealed. Herein, in-depth kinetic investigations of colorimetric detection using surface-modified Au-nanoparticle (AuNP) probes were performed for interpreting the correlation of salt concentration, reaction duration, and light absorbance. To envision these undisclosed issues, modification of AuNP surfaces with ascorbic acid was found to be highly essential for boosting the detection sensitivity due to adjusting the zeta potential of AuNP colloids towards a slightly positive value. Next, modeling the light absorbance of AuNPs under various aggregation circumstances was employed, which visually elucidated the color change so that it was visible to the naked eye, due to the intense field localization on the edges of aggregated AuNPs. In addition, the involved activation energy of AuNP aggregation was found to follow the first-order Arrhenius formula, with the extracted value of 22.5 kJ mol^{-1}. Finally, quantitative visualization of colorimetric Na^+ ion sensing was realized, and the experimental relation was obtained for explicitly determining the unknown concentration of Na^+ ions in a visual manner.

1. Introduction

Sodium ions, one of the main cations in biological systems, play an important role in the human body. In order to regulate bodily functions, such as blood pressure control, osmotic equilibrium, and pH balance, appropriate sodium salt intake is essentially required. For example, the sodium ion is an essential electrolyte for generation of action potentials in the nervous and cardiac systems. A significant effect on the variation of action potentials results from the concentration gradient for sodium ions of the cellular membrane, which correlates with cell-to-cell communication.[1,2] Sodium intake mainly occurs through the consumption of sodium in food and the sodium chloride in table salt. The American Heart Association recommends no more than 2.3 grams of sodium for an adult per day. Nevertheless, excess sodium concentration could lead to a high risk of heart attack, high blood pressure, and kidney disease, and, in extreme cases, could even result in death. Therefore, there is a high demand for instant, reliable, and sensitive detection of sodium ion concentration.

In recent years, there has been extensive exploration on methods of analysis of sodium ions (Na^+), and methods such as thermometric titration, atomic absorption spectroscopy, chromatography, and inductively coupled plasma mass spectrometry have been employed.[3–5] However, the above-mentioned methods require either expensive apparatus or complicated analysis. Moreover, practical detection remained time-consuming, with no available method to allow simple readout of the data with the naked eye. For this aspect, colorimetric methods possess the advantages of simplicity without the requirements for either complicated instrumentation or much knowledge of the electron or energy transfer involved in electrochemical or fluorescent systems, which could satisfactorily meet the requirements for practical use.

The strategy for realizing the colorimetric detection of metal ions is based on the effect of localized surface plasmon resonance (LSPR), which is a remarkable characteristic of gold nanoparticles (AuNPs), and describes the optical phenomenon produced by light waves confined within metallic particles smaller than the wavelength of the incident light.[6–8] When nanoparticles interact with incident light, surface electrons are excited by electromagnetic radiation and form surface plasmons, which spectrally reflect the maximum light absorption due to collective oscillations as the wavelength corresponds to resonant frequency.[9]

[a]*Department of Materials Science and Engineering, National Cheng-Kung University, Tainan 701, Taiwan. E-mail: timcychen@mail.ncku.edu.tw*

[b]*Hierarchical Green-Energy Materials (Hi-GEM) Research Centre, National Cheng Kung University, No. 1 University Road, Tainan 701, Taiwan*

† Electronic supplementary information (ESI) available. See https://doi.org/10.1039/d2na00211f

In 2016, detection of sodium ions was demonstrated using AuNPs as sensing probes for evaluating the concentration of Na^+ ions by colour change.[10] While the idea has been adopted to examine the hydration level in artificial sweat, the underlying critical kinetic dependence on reaction temperature and response time has not yet been revealed. In addition, Na^+ ion detection can be also realized with a plasticized PVC-based cation-selective optode system,[11] whereas the developed system strictly relied on the complicated synthesis of an ionophore-doped plasticized PVC membrane. Na^+ ions in serum can also be detected based on the G-quadruplex conformation strategy with an achievable detection limit of 0.6 μM,[12] but, thus far, there have been no further discussions on environmental influences such as reaction temperature, pH, and illumination circumstances.

Recently, gold nanomaterials were used as colorimetric probes for analysing sodium chloride in seawater, although further explorations of sensitivity dependence on analyte radius and charge have not been reported.[13] Very recently, the employment of a microfluidic colorimetric analysis system for detecting sodium benzoate was presented, where the involved colour variation was modelled with linear expression with respect to the analyte concentration featuring the sound determination coefficient of $R^2 = 0.997$.[14] Unfortunately, it was necessary for the colorimetric reaction to be initiated at 120 °C, which is a major disadvantage for its practical utilization.

In the current study, explorations of colorimetric Na^+ ion detection were carried out while taking into account the radius and charge of target analytes, pH environment, and temperature dependence using surface-functionalized AuNP probes. From in-depth kinetic examinations of AuNP aggregation phenomena, we derived information regarding the experimentally determined activation energy that accounted for the capabilities of visual Na^+ ion detection. In addition, we further discuss the quantitative modelling of light absorbance, analyte concentration, and reaction duration.

2. Experimental

2.1. Preparation of functionalized gold nanoparticles

Briefly, 0.02 M of chloroauric acid ($HAuCl_4$) was dissolved in 20 mL deionized (DI) water under gentle magnetic stirring for 1 h, and the obtained mixture was then heated at 100 °C for 15 min. After that, 0.03 g of trisodium citrate was added to the aqueous solution at 100 °C under magnetic stirring for 15 min, which resulted in the formation of dispersed AuNPs that were wine red in color.[15,16] In this reduction method, trisodium citrate acted with dual functionality for not only initiating the reduction of the $HAuCl_4$ precursors, but further functioning as a capping agent to prevent aggregation of the as-formed AuNPs. For functionalizing the AuNP surfaces, 0.2 g ascorbic acid was gently added to 20 mL of DI water, and the as-prepared solutions were subsequently mixed with the same volume of a solution of dispersed AuNPs at room temperature under gentle magnetic stirring for 30 min. The obtained surface-modified AuNPs were highly stable and could be readily preserved in the ambient condition for more than 3 months.

2.2. Characterizations

Crystallographic patterns of obtained samples were characterized with an X-ray diffractometer (Bruker AXS GmbH) using Cu-K radiation. Microstructures and diffraction patterns were investigated with transmission electron microscopy (TEM; JEM-2100F). Elemental compositions and chemical states of samples were characterized with X-ray photoelectron spectroscopy (XPS; PHI 5000 Versa Probe). Surface features of samples were analysed with a Fourier transform infrared (FTIR) spectrometer (PerkinElmer Frontier), where the measured spectra were recorded from 400 to 4000 cm^{-1}. Light absorption spectra and evaluations of colorimetric detection were measured with a UV-Vis-NIR spectrophotometer (UV-Vis; Hitachi U-3900H). Analysis of particle size and correlated zeta potential in aqueous solutions was performed with a dynamic light scattering (DLS) spectrometer (Malvern Zetasizer Nano Series).

3. Results and discussion

3.1. Characterizations of surface-modified AuNP probes

Fig. 1 presents the XRD pattern of synthesized AuNPs, where the existence of characteristic diffraction peaks corresponding to the crystallographic patterns of (111), (200), (220), and (311) of the FCC lattice were found.[17] This suggested that AuNPs with a satisfactory crystallite configuration were synthesized with a facile reduction method. The correlated microstructures were examined with TEM investigations, as shown in Fig. 1b. From viewing the diffraction patterns obtained from selectively imaging the diffracted signals at the back focal plane of an objective lens, the (111), (200), (220), and (311) planes of Au lattice could be identified, as depicted in the inset of Fig. 2b. Moreover, HRTEM characterizations were performed, where the distinct fringe spacing of 0.235 nm and 0.204 nm

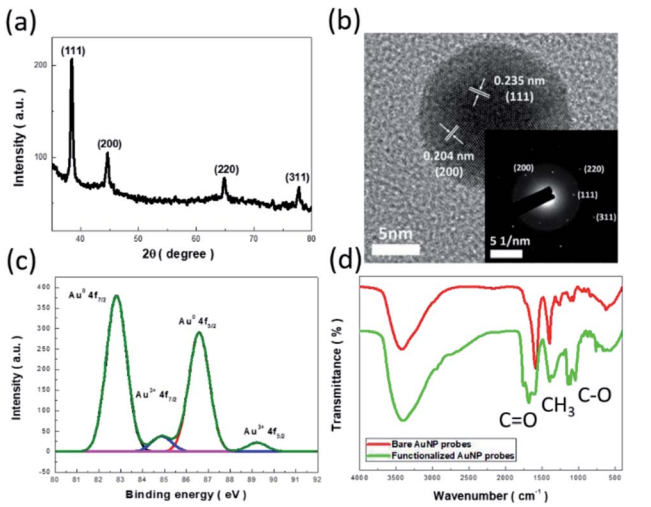

Fig. 1 (a) XRD pattern, (b) HRTEM image, and (c) XPS result of synthesized AuNPs. The diffraction pattern of a representative AuNP is presented in the inset of (b). (d) FTIR results of bare and surface-functionalized AuNPs.

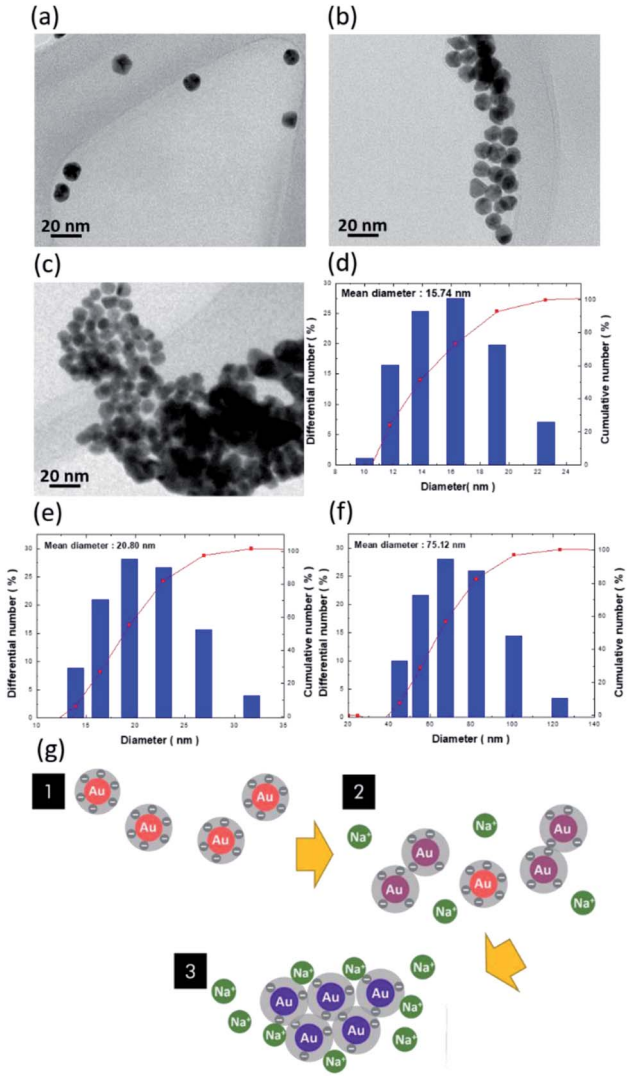

Fig. 2 Representative TEM investigations of (a) bare AuNPs, (b) mixed AuNPs/NaCl (10 mM), and (c) AuNPs/NaCl (60 mM), where the different aggregation characteristics could be validated. DLS analysis for evaluating the diameter of AuNP clusters in the presence of various NaCl concentrations: (d) 0 mM, (e) 10 mM, and (f) 60 mM and (g) schematic colloidal phenomena of AuNPs in the presence of Na^+ ions.

corresponding to crystallographic (111) and (200) was envisioned, respectively, as shown in Fig. 2b.

All these microstructural findings indicated the presence of FCC crystals of the synthesized AuNPs, which corresponded well to the results of the XRD analysis. In addition, the chemical states of as-prepared AuNPs were investigated with XPS analysis,[18,19] as presented in Fig. 1c. The dominant peaks associated with the Au $4f^{7/2}$ and $4f^{5/2}$ signals were found in spectral identification, indicating the successful reduction of $HAuCl_4$ precursors mediated with trisodium citrate as the reducing agent. The comparably weak Au^{3+} signals correlated with $4f^{7/2}$ and $4f^{5/2}$ orbitals were also displayed in the resulting photoelectron spectrum, which might have originated from the existence of a small portion of Au^{3+} complex or residual $HAuCl_4$ precursors.

Additionally, by functionalizing AuNPs with ascorbic acid, abrupt variation of surface features was found from FTIR characterizations, as shown in Fig. 1d. The measured spectra of AuNPs prior to and after functionalization by ascorbic acid are displayed, where the substantial enhancement of absorption dips spectrally as 1753–1686 cm^{-1} and 1140–1109 cm^{-1}, which corresponds to the C=O and C–O vibration modes that exist in the functionalized AuNPs, respectively, and serves as evidence of the successful modification of the AuNP surfaces.[20]

To investigate the morphological transition of colloidal AuNPs in the presence of Na^+ ions, TEM characterizations of bare AuNPs (Fig. 2a), mixed AuNPs/NaCl (10 mM) for 10 s (Fig. 2b), and AuNPs/NaCl (60 mM) for 10 s (Fig. 2c) were examined. The dispersive nature of AuNPs can be attributed to the existence of negative charges on AuNP surfaces that caused the repulsive force between neighbouring AuNPs, as evidenced in Fig. 2a, where the involved surface charges and dispersion stability are discussed later. With the addition of 10 mM Na^+ ions, dramatic agglomeration of AuNPs occurred by breaking the natural repulsion barrier. These findings were further elucidated by DLS measurements, which showed that the average dimension of AuNP clusters varied from 15.74 nm (Fig. 2d) to 20.80 nm (Fig. 2e).[21] It should be noted that insufficient Na^+ ions caused the broad distribution of cluster size, which was due to the coexistence of agglomeration and separation states of the AuNPs. At higher concentrations of Na^+ ions (60 mM), complete agglomeration of AuNPs is visible in the TEM image, as shown in Fig. 2c, where the cluster size significantly increased to 75.12 nm, as calculated in Fig. 2f.

The involved variation of colloidal phenomena is interpreted in Fig. 2g. The electrostatic repulsion between neighbouring AuNPs because of the negative surface charges was the force that maintained their dispersion in the tested solutions. With regard to the associated interaction between AuNPs responding to the variation in cluster size, there existed three main interactive forces affecting the stability of colloidal AuNPs: van der Waals force, electrostatic repulsion, and steric repulsion.[22–24] Above all, the stability of colloids composed of charged particles can be conceptually explained by the Derjaguin–Landau–Verwey–Overbeek (DLVO) theory.[25] According to the DLVO theory, the colloidal stability is determined by the balance between the van der Waals attraction forces and the electrostatic repulsion forces, where the former correlates with an attraction of intermolecular forces generated by electric dipoles, and the latter is due to the electric double layer repulsion between neighbouring AuNPs. Accordingly, the sum of the two interactions dominantly manipulated the colloidal stability of dispersing AuNPs.[22,24]

Examinations to determine the average zeta potential of AuNP probes with the addition of different concentrations of Na^+ ions are displayed in the ESI.† They indicate that the average zeta potential of the bare AuNPs without surface modification was approximately −87.7 mV. The correlated value of AuNPs treated with ascorbic acid shifted to −58.2 mV because of the obvious reduction of the negative charges on the AuNP surfaces, whereas they remained well-dispersed in the aqueous solutions. Additionally, when adding Na^+ ions, the negative surface charges were gradually suppressed, and, in turn, induced the aggregation of AuNPs due to a reduction in

the diffusion double layer's thickness with increasing ionic strength, as explained by the electrical double layer theory.[26]

Furthermore, we attempted to introduce surface functionalization with ascorbic reagents to slightly shift the energy balance of particle colloidality toward reducing the particle spacing. This could accelerate the detection of Na^+ ions to achieve increased sensitivity. A colorimetric table for detecting Na^+ ions from AuNP probes without surface functionalization, which resulted in suppressed detection rates, is presented in the ESI.†

The optical characteristics of the AuNP probes in the presence of Na^+ ions are displayed in Fig. 3a. Systematic investigations of light-absorption spectra upon varying the detection durations from 0 to 900 s in the presence of a similar salt concentration of 45 mM were monitored. In the case of 0 s, *i.e.*, dispersed solutions of bare AuNPs, the maximum absorbance of surface-modified AuNP probes was centred at 525 nm, which was attributed to the LSPR effect of AuNPs responding to the strong light absorption contributed by the collective oscillation of free electrons. The spectral position of light absorbance shifted to a long wavelength regime when Na^+ ions were introduced, and, therefore, the absorption peak was red-shifted from approximately 600 nm (30 s) to 690 nm (600 s). Additionally, the absorbance intensities were decreased accordingly, which originated from the agglomeration of AuNPs. This was followed by a reduction in AuNP density, which reflected a decrease in the number of active sites that could absorb the incoming light.

The measured absorption spectra under various Na^+ concentrations were further modelled with the finite-difference time-domain (FDTD) calculation (Fig. 3b),[27–29] where different aggregation conditions of AuNPs were considered to spectrally fit the measured data for providing the elucidative picture of correlated LSPR effects, as detailed in the ESI.† A similar shift in the absorption spectra associated with aggregation conditions of AuNPs (simulated results) in correlation with the duration of AuNP/Na^+ interaction (experimental results) verified that the *in situ* microscopic phenomena could be qualitatively monitored with FDTD calculation. It should be noted that the slightly broader absorption spectra were calculated as compared to measured data, which could be attributed to the instrumental limitation of detecting all the scattering lights with the finite size of the aperture in the UV/Vis spectrometer.

To explore the spatial distribution of light-absorption sites when LSPR effects were encountered under various conditions of AuNP agglomeration, the field mappings of AuNPs at the wavelength of the central absorption peak were monitored, as shown in Fig. 3c. The comparative results clearly indicated that the field distributions were resonantly localized at regions of AuNP surfaces under isolated, well-dispersed states (Fig. 3c), and at the edges of overlapping regions of neighbouring AuNPs (Fig. 3d–f), while the intensity of the field localization in the case of the latter seemed to be substantially greater than that of the former.

These features explained the phenomena observed with the naked eye, where the present colour of the AuNP indicators became darker (from red to purple to dark grey) as greater numbers of AuNPs were aggregated even though the overall absorption intensities were reduced, as evidenced in the measured and calculated spectra (Fig. 3a and b). Examinations of average zeta potential indicated that the main mechanism for AuNP aggregation could be attributed to the shift of the average zeta potential toward the positive regime when adding Na^+ ions, which subsequently caused the instant color variations of AuNPs, depending on the extent of AuNP aggregation.

To explore the potential sensing capability of AuNP probes functioning as colorimetric indicators, visual examination of Na^+ ion detection is presented in Fig. 4a.[30,31] The color of the AuNP solutions gradually changed from red to purple, and even to dark grey, due to the obvious agglomeration of the AuNPs. It should be noted that the involved colorimetric detection could be repetitively utilized by transforming the aggregation state to the recovery of dispersed conditions, as demonstrated in the ESI.†

The reaction times of colour variations decreased as the salt concentrations were increased. Furthermore, the minimum concentration that could be visually detected through the naked eye was found to be approximately 30 mM, which only required 30 s to reach an obvious colour change. The time required for visual detection was unambiguously decreased while the tested salt concentration was increased. The colour change of the AuNPs remarkably decreased to less than 5 seconds at 60 mM, providing an instant and reliable detection strategy for sodium salts.

To further quantitatively visualize the colour change, the corresponding colour distributions in the presence of various salt concentrations were numerically displayed with the standard CIE colour space,[30] as shown in Fig. 4b. *X* and *Y* values, corresponding to the normalization of the tri-stimulus values in the two-dimensional spatial domain of colour space, clearly indicated that the trends of time-dependent colour variation in the presence of different salt concentrations were distinct. Specifically, the approximately straight and steeply curved variations of *X* and *Y* values in the chromaticity diagrams in the case of low (30 mM, left diagram) and high (45 mM, right

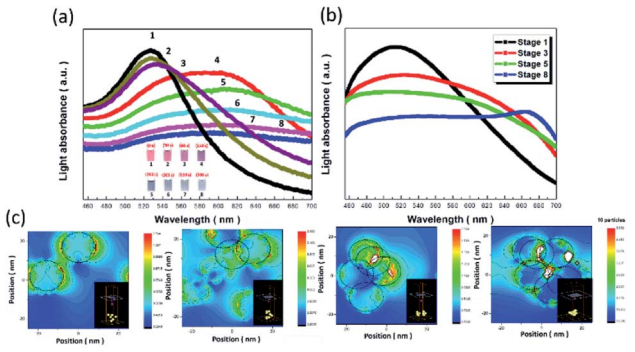

Fig. 3 (a) Measured and (b) simulated absorption spectra of AuNP probes upon varying detection durations from 0 to 900 s in the presence of the same salt concentration of 45 mM. (c) Distribution of an electric field under various conditions of AuNP aggregation, where the correlated examinations of aggregation conditions of AuNP are shown in the inset figures, respectively.

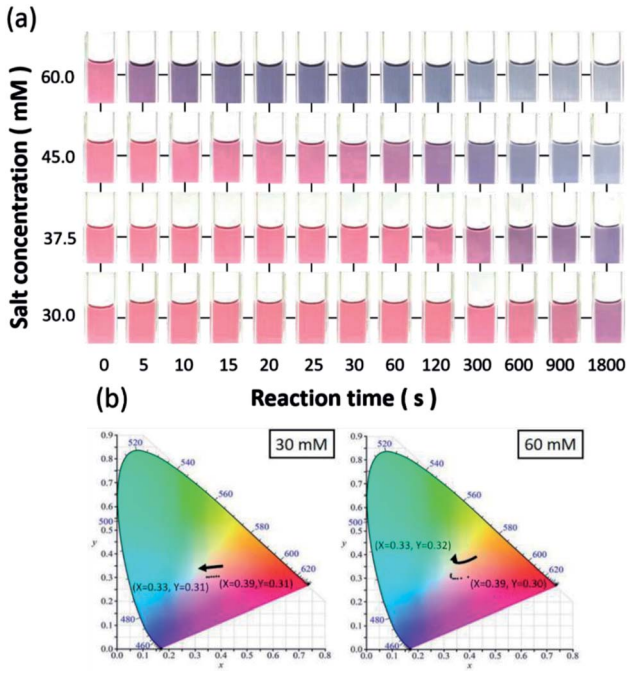

Fig. 4 (a) Visual colorimetric table of Na^+ ion detection under various salt concentrations and reaction durations. CIE chromaticity diagrams of AuNP probes in the presence of (b) 30 mM (left diagram) and 60 mM (right diagram) of sodium salts.

diagram) salt concentrations with respect to the elongation of reaction time are displayed in Fig. 4b.

These results provide an intuitive vision of the dynamic change of indicator colour depending on the salt concentration and reaction time, which were in good agreement with the colorimetric table shown in Fig. 4a. In addition to the employment of CIE colour space, the commercially used RGB colour model was also employed as an alternative to examine the involvement of colour change. It validated the fact that the change in red colour space with respect to reaction time was predominant in three examined color spaces that responded to the detection of salt concentration, as shown in the ESI.†

3.2. Effect of ion radius and charge on colorimetric detection

As discussed in Fig. 2, the colour change of the AuNP probes resulted from the nature of the colloid aggregation of AuNPs, which might be influenced by determined factors, including analyte features, environmental pH, and reaction temperature. Fig. 5a displays a colorimetric table that takes into account the visual detection of various alkali and alkaline earth metal ions, including lithium (Li^+), potassium (K^+), magnesium (Mg^{2+}), calcium (Ca^{2+}), and strontium (Sr^{2+}) ions. The results explicitly indicate that the available colour visualization by the naked eye was influenced by the detected analytes. With the addition of cation ions in the same concentration range (15–52.5 mM), the presence of K^+ ions induced variation in the spectral LSPR effect of AuNPs more rapidly than Li^+ and Na^+ ions. Additionally, the minimum concentration of K^+ ions that could be visually detected was 15 mM, which was comparably

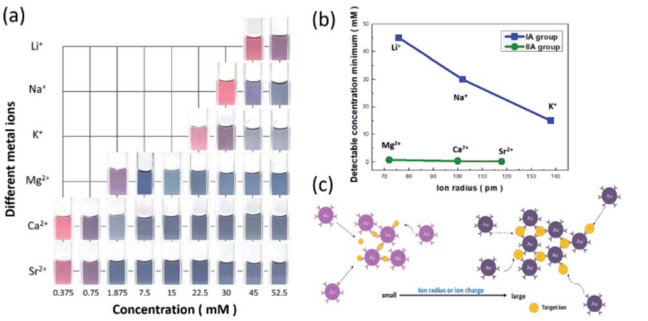

Fig. 5 (a) Comparative colorimetric examinations of AuNP probes for detecting various cation ions. (b) Plot of the detectable minimum concentration of various cation ions with respect to the corresponding ion radiuses. (c) Illustrated detection mechanism of AuNP probes influenced by ion radius and charge of target analytes.

lower than that for Na^+ (30 mM) and Li^+ (45 mM) ions, as shown in Fig. 5b. Likewise, a similar trend was found in a group of alkaline earth metal ions, where the sensing affinity followed the order of $Mg^{2+} < Ca^{2+} < Sr^{2+}$ ions (Fig. 5b), which implied that the detection sensitivity was highly affected by the cation radius.

Other than that, another determinate influence relied on cation charge, where the detection of divalent cations seemed to be more kinetically favourable for the intended aggregation of AuNPs than the sensing condition of monovalent ions, where the available minimum detection of cation ions with respect to the ion radius is displayed in Fig. 5b. As a consequence, we inferred that the detected minimum concentration of AuNP probes was inversely dependent on the product of the cube of ion charge and ion radius, as summarized in Table 1 (Fig. 5c), which illustrates the underlying correlation of two analyte features impacting the aggregation of AuNPs.

Cation ions with a larger radius provided additional active sites for contact with AuNPs, which resulted in greater availability for AuNP agglomeration. This steric effect in terms of larger cation radius favoured the rapid and efficient variation in colour visualized by the naked eye, thus reducing the detection minimum of cation concentration. However, the existence of additional surface charges on cation ions also facilitated the ionic interaction between negatively charged AuNPs and positively charged cation ions, which in turn benefited the detection sensitivity in the case of low cation concentration. In addition, the detection selectivity and practical applications, such as detecting residual Na^+ ions on chopsticks using AuNP probes as indicators, were further examined, as shown in the ESI.†

Table 1 Detection parameters of different metal ions

Metal ions	Ion radius (pm)	(Ion charge)^3 × ion radius	Detectable concentration minimum (mM)
Li^+	76	76	45
Na^+	102	102	30
K^+	138	138	15
Mg^{2+}	72	288	0.75
Ca^{2+}	100	800	0.37
Sr^{2+}	118	944	0.2

3.3. Effect of pH value on protonation of AuNPs

A colorimetric table for detecting Na^+ ions with the adjustment of pH is shown in Fig. 6a. The observed colour change *versus* reaction time was greatly reduced when the pH value decreased, while the colour of the AuNP probes was readily altered to be purple in the case of pH 1.5. These findings suggest that the protonation of AuNPs essentially dominated the succeeding aggregation due to the suppression of negative charges on the AuNPs at pH 1.5.[32,33] This implied that the AuNPs might lose their detection capability under such circumstances because they directly entered the aggregation stage prior to initiating the informative visual sensing of analytes.

The involved protonation of AuNPs due to the variation in environmental pH can be further evidenced by the measurement of corresponding zeta potentials, as shown in Fig. 6b. The aqueous zeta potentials shifted to higher values when the pH values were reduced under three various concentrations of sodium salt, which implies that the inherently negative polarity of AuNP surfaces with negative charges were partially identified due to encountering protonation mediation through lowering of the environmental pH values. Apart from that, the designed AuNP probes remained active and efficient under a wide pH range from 3 to 9.5 (Fig. 6a), which could meet the requirements for practical employment to detect salt. Moreover, from examining the change in the average zeta potentials under three different salt concentrations, it was observed that the corresponding values of zeta potential were maintained in a narrow range under pH = 3–9.5, where the deviations in the zeta potential were less than 16% (for salt concentration of 30.0 mM), 10% (for salt concentration of 37.5 mM), and 8% (for salt concentration of 45.0 mM), which thus validated the sensor stability for detecting Na^+ ions.

3.4. Effect of temperature on sensor stability and reaction kinetics

The employment of a colorimetric sensor essentially requires wide thermal durability for stable detection of the target analytes against thermal fluctuation from environmental conditions. Fig. 7 presents systematic investigations of the influences of temperature upon the colorimetric detection capability of

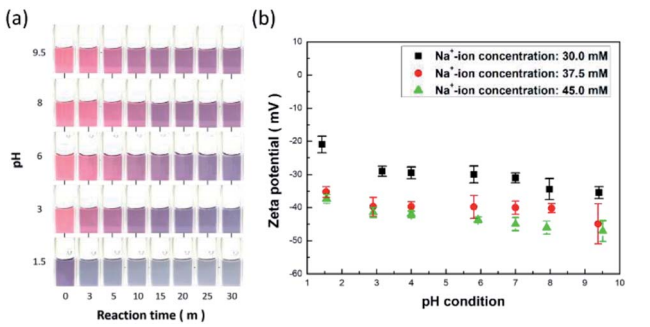

Fig. 6 (a) Colorimetric examinations of Na^+ ions under various pH conditions. (b) Measured zeta potentials of analyte solutions in the presence of Na^+ ions with concentrations of 30.0, 37.5, and 45.0 mM under different pH values.

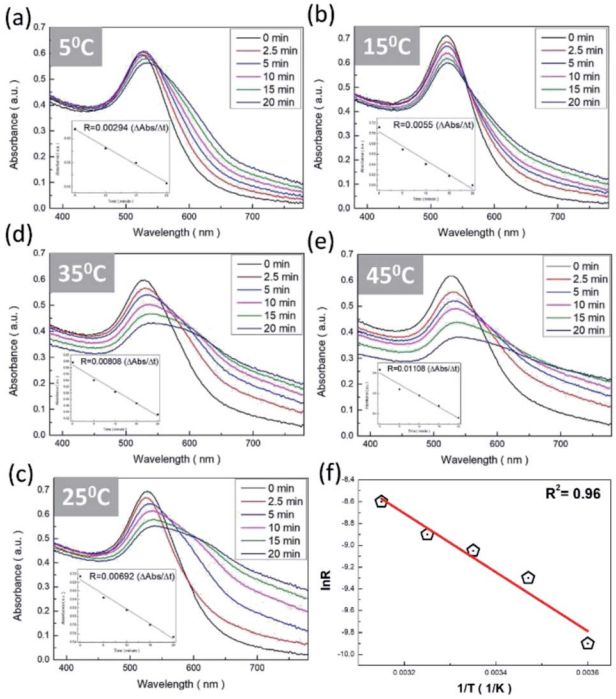

Fig. 7 Colorimetric sensitivity tests of Na^+ ions under various environmental temperatures: (a) 5 °C, (b) 15 °C, (c) 25 °C, (d) 35 °C, and (e) 45 °C. (f) Correlation of rate constants in natural logarithm form and corresponding inverse temperatures. The linear regression possessed the R^2 of 0.96.

AuNP probes. By examining the light absorbance in the vicinity of spectral LSPR position (380–780 nm) with the addition of sodium salt (37.5 mM), variations in the spectral absorbance of AuNP probes with respect to the reaction durations (0–20 min) were monitored at environmental temperatures of 5 °C (Fig. 7a), 15 °C (Fig. 7b), 25 °C (Fig. 7c), 35 °C (Fig. 7d), and 45 °C (Fig. 7e).

To quantitatively explore the correlated thermodynamic kinetics, a plot of absorbance variation, determined by the change in the average absorbance within the wavelength of 380–780 nm and relative to reaction durations at each environmental temperature, was characterized for extracting the rate constant corresponding to the kinetic features of colorimetric phenomena, as shown in the insets of Fig. 7. The results clearly indicate the positive correlation between the temperature-dependent rate constant and environmental temperature. This provided elucidation regarding the rate-determining step for the involved colorimetric characteristics, which was colloidal aggregation accompanying the thermally driven activation energy that resulted in varying amounts of AuNP coalescence. To gain further insight into the involvement of activation energy on AuNP aggregation, the Arrhenius equation was adopted, as shown below:[34]

$$R = A \exp\left(\frac{-E_a}{RT}\right) \quad (1)$$

where R denotes the measured rate constant, A denotes the pre-exponential factor, T denotes the absolute temperature, R

denotes the universal gas constant, and E_a denotes the activation energy. By considering the natural logarithm of the Arrhenius equation, the experimental correlation is expressed as below:

$$\ln R = \ln A - \frac{E_a}{R}\frac{1}{T} \quad (2)$$

where the resulting diagram in terms of $1/T$ *versus* $\ln R$ featuring zero-order reaction kinetics is presented in Fig. 7f, which shows sound linear expression with R^2 of 0.95. The detailed results are presented in Table 2. Additionally, the slope, in terms of $-E_a/R$, can be readily obtained from the linear calibration, and, thus, the activation energy was estimated to be 22.5 kJ mol^{-1}. The extracted results were comparable to those found in the literature, where Dutta *et al.* demonstrated that the activation barrier of AuNP aggregation in aqueous solution was 36.2 kJ mol^{-1} in the temperature range 20–60 °C.[35] It should be emphasized that reported investigations on the activation phenomena of the colorimetric sensing method have been rare.

In addition, the slightly lower activation energy obtained in our work could be attributed to the induced agglomeration that resulted after adding Na^+ ions that strengthened the ionic attraction between neighbouring AuNPs through overcoming the energy barrier that arose from collision hindrance and citrate desorption from AuNP surfaces. It was also found that the thermodynamic coalescence of two nanocrystallite NPs was recognized with a similar crystallographic facet on the atomic scale in order to remedy the involvement of surface free energy, which therefore contributed to either raising the temperature above ambient or decelerating the reaction rate.[36,37] Evidently, these kinetic restrictions did not take place during the AuNP-based colorimetric detection of Na^+ ions presented in this work, because the mediation of Na^+ ions readily decreased the energy barrier and facilitated ionic-force-induced aggregation by shortening the self-diffusion distance of the AuNPs.

It should be noted that the optical sensing of sodium ions could be realized by other methods, including surface-enhanced Raman scattering,[41] fluorescence techniques,[42] and photonic diffraction.[43] While their sensing capabilities were remarkably sound, the aforementioned methods require either sophisticated spectral instruments or complicated patterning fabrication that prevents their practical employment. Moreover, the developed AuNP probes for colorimetric sensing with sensitive and easily employed capabilities could be particularly utilized for on-site and instant sensing applications.

Table 2 Kinetic parameters of AuNP aggregations with respect to environmental temperatures

T (°C)	T (K)	R (a.u./min)	R (a.u./sec)	$\frac{1}{T}\left(\frac{1}{K}\right)$	$\ln R$
5	278	0.00294	0.000049000	0.003 597 122	−9.92 369 026
15	288	0.0055	0.000091666	0.003 472 222	−9.297 351 749
25	298	0.00692	0.000115 333	0.003 355 705	−9.067 684 072
35	308	0.00808	0.000134 667	0.003 246 753	−8.912 707 969
45	318	0.01108	0.000184 667	0.003 144 654	−8.59 695 816

3.5. Quantitative analysis

Quantitative examinations of salt concentration are essential for colorimetric sensing, and could provide a universal database for visually monitoring the variation in Na^+ ions.[38–40] We attempted to determine the experimental expression through the considerations of light absorbance and reaction time responding to salt concentration. Three different strategies were used for monitoring the light absorbance under varying reaction durations of AuNPs interacted with Na^+ targets, by recording the (i) absorption intensity at 525 nm, (ii) the intensity ratio of light absorbance at 600 nm to 525 nm, and (iii) the average absorption intensity at wavelengths of 380 nm to 780 nm. The results from the first two examination methods are presented in the ESI,† while the results from the third method featuring the comparably rational model are demonstrated in Fig. 8a–g.

The underlying reason behind the rationality of this strategy could be associated with the fact that the spectral variations in light absorbance were quite broad, from 380 nm to 780 nm,

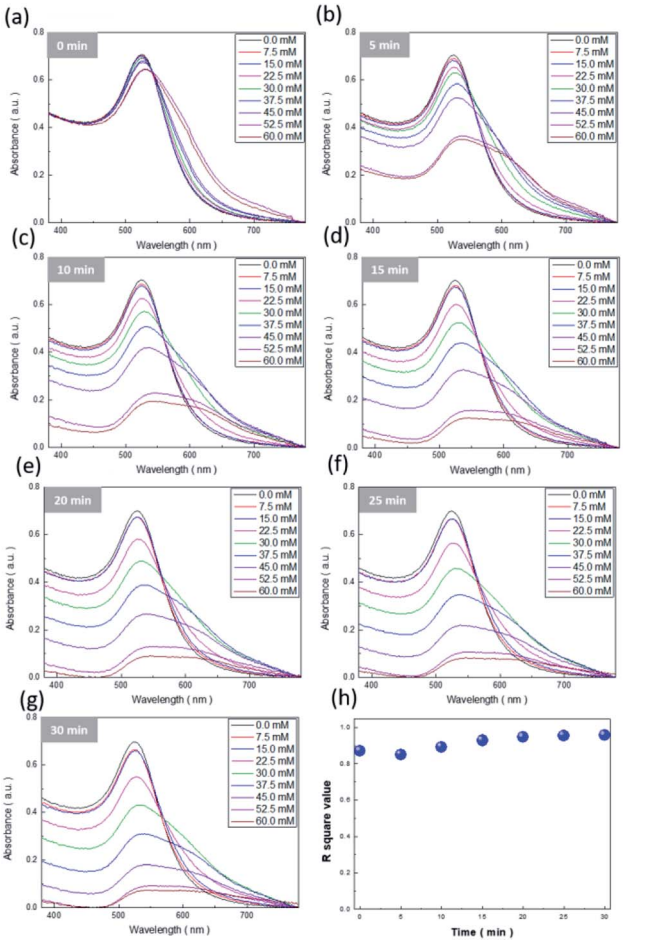

Fig. 8 Colorimetric sensitivity tests of Na^+ ions with various concentrations from 0 to 60 mM under different reaction durations: (a) 0 min, (b) 5 min, (c) 10 min, (d) 15 min, (e) 20 min, (f) 25 min, and (g) 30 min. (h) Correlation of R^2 values extracted from the linear regression of the measured results presented in (a–g), with respect to various reaction durations.

while the reaction durations were longer than 15 min (Fig. 8d–g). Thus, similar to the treatment presented in the insets of Fig. 7, linear regression by fitting the correlation between average light absorbance and salt concentration was employed to examine the results under the variation of reaction time from 0 to 30 min, with 5 min as each interval, and where the corresponding R^2 values of linear fitting with respect to the reaction duration are envisioned in Fig. 8h. Clearly, the corresponding R^2 values were maintained above 0.96 regardless of detection time, which explicitly provided a reliable analysis of the light-absorption phenomena of AuNPs for detecting Na^+ ions covering a large timespan. On the basis of these established models, the correlated mathematical expression was further explored *via* the employment of the second-order polynomial regression:

$$\text{Response (light absorbance)} = 0.74 + 2.1 \times 10^{-3} C_{Na^+} - 8.5 \times 10^{-3} t - 3.3 \times 10^{-4} C_{Na^+} t - 9.9 \times 10^{-5} C_{Na^+}{}^2 + 3.310^{-4} t^2 \quad (3)$$

where the correlated R^2 value of the applied second order polynomial regression was approximately 0.97, revealing the sound experimental relation that can be employed to estimate the unknown concentration of Na^+ ions by considering the light absorbance and reaction time in a quantitative manner.

4. Conclusions

The employment of ascorbic-acid-treated AuNP probes enabled activation of pronounced colour changes for visually detecting quantities of Na^+ ions. These features were facilitated by adjusting the zeta potential of AuNP colloids towards a slightly positive value, which resulted in AuNP aggregation due to the ionic interaction between negatively charged AuNPs and positively charged sodium ions. More importantly, we found that the ionic radius and charge of the target, pH, and environmental temperature contributed remarkable impacts upon the sensing speed as well as detection of the minimum concentration. The quantitative visualization of colorimetric Na^+ ion sensing was performed through gaining an experimental relation that could be finely employed to estimate the unknown concentration of Na^+ ions by considering the light absorbance and reaction duration. The colorimetric sensing investigated here not only exhibited efficient, sensitive, and easily employed capabilities, but further unveiled the practical impacts on detection kinetics. These factors might provide a potential method for *in situ* sensing of biomolecules using other visual biomedical devices.

Conflicts of interest

There are no conflicts to declare.

Acknowledgements

This work was supported by the Ministry of Science and Technology of Taiwan (MOST 110-2223-E-006-003-MY3), and the Hierarchical Green-Energy Materials (Hi-GEM) Research Center, from The Featured Areas Research Center Program within the framework of the Higher Education Sprout Project by the Ministry of Education (MOE) and the Ministry of Science and Technology (MOST 111-2634-F-006-008) in Taiwan. The authors greatly thank the Core Facility Center at National Cheng Kung University for the facilities provided for conducting material characterizations.

Notes and references

1 R. K. Orkand and R. Niedergerke, Heart action potential: Dependence on external calcium and sodium ions, *Science*, 1964, **146**, 1176–1177.
2 M. P. Blaustein, Sodium ions, calcium ions, blood pressure regulation, and hypertension: a reassessment and a hypothesis, *Am. J. Physiol.*, 1977, **232**, C165–C173.
3 Q. Ye, Q. Li, Q. Lv, Y. Li and Y. Gong, Determination methods of sodium ion in food, *J. Food Saf. Food Qual.*, 2016, **7**, 4576–4580.
4 M. Chamsaz, M. H. Arbab-Zavar, A. Darroudi and T. Salehi, Preconcentration of thallium (I) by single drop microextraction with electrothermal atomic absorption spectroscopy detection using dicyclohexano-18-crown-6 as extractant system, *J. Hazard. Mater.*, 2009, **167**, 597–601.
5 P. Yan, M. He, B. Chen and B. Hu, Restricted accessed nanoparticles for direct magnetic solid phase extraction of trace metal ions from human fluids followed by inductively coupled plasma mass spectrometry detection, *Analyst*, 2015, **140**, 4298–4306.
6 F. Hao, Y. Sonnefraud, P. VanDorpe, S. A. Maier, N. J. Halas and P. Nordlander, Symmetry breaking in plasmonic nanocavities: subradiant LSPR sensing and a tunable Fano resonance, *Nano Lett.*, 2008, **8**, 3983–3988.
7 K. Y. Kuo, S. H. Chen, P. H. Hsiao, J. T. Lee and C. Y. Chen, Day-night active photocatalysts obtained through effective incorporation of Au@ CuxS nanoparticles onto ZnO nanowalls, *J. Hazard. Mater.*, 2022, **421**, 126674.
8 M. Condorelli, L. Litti, M. Pulvirenti, V. Scardaci, M. Meneghetti and G. Compagnini, Silver nanoplates paved PMMA cuvettes as a cheap and re-usable plasmonic sensing device, *Appl. Surf. Sci.*, 2021, **566**, 150701.
9 C. Deng, F. Chen, C. Liu, Q. Liu, K. Chen, C. Zou, Z. Zhao, Y. Zhu, X. Wang and F. Gao, Realization of Specific Localized Surface Plasmon Resonance in Au-Modified Ni Nanoplasmonics for Efficient Detection, *Appl. Surf. Sci.*, 2022, 152288.
10 Y. Zhou, H. Han, H. P. P. Naw, A. V. Lammy, C. H. Goh, S. Boujday and T. W. J. Steele, Real-time colorimetric hydration sensor for sport activities, *Mater. Des.*, 2016, **90**, 1181–1185.
11 H. Shibata, T. G. Henares, K. Yamada, K. Suzuki and D. Citterio, Implementation of a plasticized PVC-based cation-selective optode system into a paper-based analytical device for colorimetric sodium detection, *Analyst*, 2018, **143**, 678–686.
12 H. Sun, H. Chen, X. Zhang, Y. Liu, A. Guan, Q. Li, Q. Yang, Y. Shi, S. Xu and Y. Tang, Colorimetric detection of

sodium ion in serum based on the G-quadruplex conformation related DNAzyme activity, *Anal. Chim. Acta*, 2016, **912**, 133–138.

13 T. Mbambo, S. C. Onwubu, P. S. Mdluli and L. M. Madikizela, Development of a gold nanomaterial enabled colorimetric sensor method for the analysis of sodium chloride in seawater, *Environ. Nanotechnol., Monit. Manage.*, 2019, **12**, 100275.

14 H. Ko, C. C. Liu, K. H. Chen, F. Sheu, L. M. Fu and S. J. Chen, Microfluidic colorimetric analysis system for sodium benzoate detection in foods, *Food Chem.*, 2021, **345**, 128773.

15 S. Wang, A. A. Rogachev, M. A. Yarmolenko, A. VRogachev, J. Xiaohong, M. S. Gaur, P. A. Luchnikov, O. VGaltseva and S. A. Chizhik, Structure and properties of polyaniline nanocomposite coatings containing gold nanoparticles formed by low-energy electron beam deposition, *Appl. Surf. Sci.*, 2018, **428**, 1070–1078.

16 C. Y. Chen, L. J. Hsu, P. H. Hsiao and C. T. R. Yu, SERS detection and antibacterial activity from uniform incorporation of Ag nanoparticles with aligned Si nanowires, *Appl. Surf. Sci.*, 2015, **355**, 197–202.

17 U. T. Khatoon, G. V. S. N. Rao, M. K. Mohan, A. Ramanaviciene and A. Ramanavicius, Comparative study of antifungal activity of silver and gold nanoparticles synthesized by facile chemical approach, *J. Environ. Chem. Eng.*, 2018, **6**, 5837–5844.

18 J. Young, M. Sauer, G. M. D. M. Rubio, A. Sato, A. Foelske, C. J. Serpell, J. M. Chin and M. R. Reithofer, One-step synthesis and XPS investigations of chiral NHC–Au (0)/Au (I) nanoparticles, *Nanoscale*, 2019, **11**, 8327–8333.

19 Y. Gao, C. Xing, S. Hu and S. Zhang, In Situ exsolved Au nanoparticles from perovskite oxide for efficient epoxidation of styrene, *J. Mater. Chem. A*, 2021, **9**, 10374–10384.

20 K. Y. Kuo, S. H. Chen, P. H. Hsiao, J. T. Lee and C. Y. Chen, Day-night active photocatalysts obtained through effective incorporation of Au@CuxS nanoparticles onto ZnO nanowalls, *J. Hazard. Mater.*, 2022, **421**, 126674.

21 P. H. Hsiao and C. Y. Chen, Insights for realizing ultrasensitive colorimetric detection of glucose based on carbon/silver core/shell nanodots, *ACS Appl. Bio Mater.*, 2019, **2**, 2528–2538.

22 J. Polte, Fundamental growth principles of colloidal metal nanoparticles–a new perspective, *CrystEngComm*, 2015, **17**, 6809–6830.

23 P. Attard, Recent advances in the electric double layer in colloid science, *Curr. Opin. Colloid Interface Sci.*, 2001, **6**, 366–371.

24 J. Zhou, J. Ralston, R. Sedev and D. A. Beattie, Functionalized gold nanoparticles: synthesis, structure and colloid stability, *J. Colloid Interface Sci.*, 2009, **331**, 251–262.

25 A. Gomez-Flores, S. A. Bradford, G. Hwang, S. Choi, M. Tong and H. Kim, Shape and orientation of bare silica particles influence their deposition under intermediate ionic strength: A study with QCM–D and DLVO theory, *Colloids Surf., A*, 2020, **599**, 124921.

26 C. Burns, W. U. Spendel, S. Puckett and G. E. Pacey, Solution ionic strength effect on gold nanoparticle solution color transition, *Talanta*, 2006, **69**, 873–876.

27 S. H. Chen, T. C. Wei, T. Y. Wu and C. Y. Chen, Interface management of silicon-nanowire based hybrid solar cells through facile solution-processed oxidation, *Mater. Lett.*, 2022, **307**, 130967.

28 Q. Sun, Q. Y. Zhang, N. Zhou, L. Y. Zhang, Q. Hu and C. Y. Ma, FDTD simulation of Ag-decorated ZnO nanorods for optimization of 3D SERS substrates, *Appl. Surf. Sci.*, 2021, **565**, 150524.

29 P. H. Hsiao, Y. C. Lai and C. Y. Chen, Dual-sized carbon quantum dots enabling outstanding silicon-based photodetectors, *Appl. Surf. Sci.*, 2021, **542**, 148705.

30 Y. Jiang, H. Zhao, Y. Lin, N. Zhu, Y. Ma and L. Mao, Colorimetric detection of glucose in rat brain using gold nanoparticles, *Angew. Chem.*, 2010, **122**, 4910–4914.

31 H. A. Badran, S. J. Bader, R. K. F. Alfahed and N. A. H. Saleh, Study of Colorimetric properties of Ethidium bromide dye-doped PVP/DNA film, *J. Phys.: Conf. Ser.*, 2021, 12102.

32 B. Contreras-Trigo, V. Díaz-García, E. Guzmán-Gutierrez, I. Sanhueza, P. Coelho, S. E. Godoy, S. Torres and P. Oyarzún, Slight pH fluctuations in the gold nanoparticle synthesis process influence the performance of the citrate reduction method, *Sensors*, 2018, **18**, 2246.

33 H. He, J. Ostwaldt, C. Hirschhäuser, C. Schmuck and J. Niemeyer, Dual pH-Induced Reversible Self-Assembly of Gold Nanoparticles by Surface Functionalization with Zwitterionic Ligands, *Small*, 2020, **16**, 2001044.

34 K. J. Laidler, The development of the Arrhenius equation, *J. Chem. Educ.*, 1984, **61**, 494.

35 A. Dutta, A. Paul and A. Chattopadhyay, The effect of temperature on the aggregation kinetics of partially bare gold nanoparticles, *RSC Adv.*, 2016, **6**, 82138–82149.

36 H. L. Skriver and N. M. Rosengaard, Surface energy and work function of elemental metals, *Phys. Rev. B*, 1992, **46**, 7157.

37 J. W. Park and J. S. Shumaker-Parry, Structural study of citrate layers on gold nanoparticles: role of intermolecular interactions in stabilizing nanoparticles, *J. Am. Chem. Soc.*, 2014, **136**, 1907–1921.

38 Z. Yan, S. Guang, H. Xu and X. Liu, An effective real-time colorimetric sensor for sensitive and selective detection of cysteine under physiological conditions, *Analyst*, 2011, **136**, 1916–1921.

39 X. Liu, X. Wang, C. Qi, Q. Han, W. Xiao, S. Cai, C. Wang and R. Yang, Sensitive colorimetric detection of ascorbic acid using Pt/CeO_2 nanocomposites as peroxidase mimics, *Appl. Surf. Sci.*, 2019, **479**, 532–539.

40 K. Ellerbee, S. T. Phillips, A. C. Siegel, K. A. Mirica, A. W. Martinez, P. Striehl, N. Jain, M. Prentiss and G. M. Whitesides, Quantifying colorimetric assays in paper-based microfluidic devices by measuring the transmission of light through paper, *Anal. Chem.*, 2009, **81**, 8447–8452.

41 P. A. Mosier-Boss, Review of SERS substrates for chemical sensing, *Nanomaterials*, 2017, **7**(6), 142.

42 X. Liu, S. Tao, N. Deng, Y. Liu, B. Meng, B. Xue and G. Liu, Synchronous-scan fluorescence as a selective detection method for sodium dodecylbenzene-sulfonate and pyrene in environmental samples, *Anal. Chim. Acta*, 2006, **572**(1), 134–139.

43 A. K. Yetisen, Y. Montelongo, M. M. Qasim, H. Butt, T. D. Wilkinson, M. J. Monteiro and S. H. Yun, Photonic Nanosensor for Colorimetric Detection of Metal Ions, *Anal. Chem.*, 2015, **87**(10), 5101–5108.